Technical note on the measurement of inspiral higher order modes by coherentWaveBurst in GW190814

G. A. Prodi[a,b,*], G. Vedovato[c,*], M. Drago[d,e], S. Klimenko[f], C. Lazzaro[g,c], A. Miani[a,b], E. Milotti[h], F. Salemi[i], S. Tiwari[j]

[a] *Università di Trento, Dipartimento di Matematica, I-38123 Povo, Trento, Italy*
[b] *INFN, TIFPA, I-38123 Povo, Trento, Italy*
[c] *INFN, Sezione di Padova, I-35131 Padova, Italy*
[d] *Gran Sasso Science Institute, Via F. Crispi 7, I-67100, L'Aquila, Italy*
[e] *INFN, Laboratori Nazionali del Gran Sasso, I-67100 Assergi, Italy*
[f] *University of Florida, Gainesville, FL 32611, USA*
[g] *Università di Padova, Dipartimento di Fisica e Astronomia, I-35131 Padova, Italy*
[h] *Dipartimento di Fisica, Universit'a di Trieste and INFN Sezione di Trieste, Via Valerio, 2, I-34127 Trieste, Italy*
[i] *Università di Trento, Dipartimento di Fisica, I-38123 Povo, Trento, Italy*
[j] *Physik-Institut, University of Zurich, Winterthurerstrasse 190, 8057 Zurich, Switzerland*

Executive Summary

The detection and waveform reconstruction of gravitational wave transients on LIGO-Virgo data is pursued by a variety of methods, either exploiting detailed signal models or using minimal assumptions on the signal morphology [1]. The coherentWaveBurst (cWB) pipeline [2] provides well established methods both for the detection and for the reconstruction of transient signals, based on a waveform agnostic search for a coherent response in the network of detectors, implemented in time-frequency domain by exploiting the Wilson-Daubechies-Meyer (WDM) wavelet transform [3]. Here we present a recently developed analysis procedurs based on cWB, targeting the detection of spectral features beyond the quadrupolar emission in the inspiral phase of compact binary coalescences. This method has been used in the GW190814 discovery paper [4] and is an evolution of the methods already described in [5]. The main underlying idea is to compare the waveform agnostic signal reconstruction provided by cWB to the predictions provided by coherent Bayesian inference exploiting detailed waveform models [6, 7]. In order to target undertones or overtones of the main quadrupolar emission, the test of consistency is performed within suitable chirp-like slices of the time-frequency representation of the event. The choice of these time-frequency slices is driven by a mild optimization of the Receiver Operating Characteristic (ROC), see e.g. [8]. The GW190814 results presented in [4] are discussed in more depth, providing supplemetary material both on the evidence for the $m = 3$ mode and for the interpretation of the multiple tests of waveform consistency performed over a wide range of chirping undertones and overtones.

*Corresponding authors

Email addresses: giovanniandrea.prodi@unitn.it (G. A. Prodi), gabriele.vedovato@lnl.infn.it (G. Vedovato)

Preprint submitted to LIGO Document T2000124 and Virgo TDS VIR-0319A-20 *April 2, 2020*

1. Introductory remarks

CoherentWaveBurst (cWB) provides a well established set of data analysis methods both for the detection and for the reconstruction of transient gravitational waves [2, 9], based on a waveform-agnostic search for a coherent response in the network of earth-based interferometric detectors. An open source release of cWB is available at https://gitlab.com/gwburst/public/library with related documentation at https://gwburst.gitlab.io/.

The goal of this technical note is to provide a description of the cWB method to detect possible undertones and overtones of the dominant quadrupolar emission described by the m=2 multipole. This is meant to supplement the related content in the GW190814 discovery paper, [4]. An alternative method is described at [10] and its results has been included both in [11] and in the GW190412 discovery paper, [4]. The more general description of the method for comparing cWB reconstructed signals with signal models obtained from Bayesian inference can be found in [5].

The scientific context and latest results on the detection of higher order modes emitted during the inspiral phase of compact binary coalescences are described in [11] and [4].

This note is organized as follows. Section 2 recalls the main steps of the waveform comparison procedure and the definition of the test statistic, i.e. the waveform residual energy. Section 3 describes the choice of the relevant time-frequency portion (slice) where the waveform residual energy is evaluated. Section 4 focuses on the interpretation of the cWB results and discusses some relevant checks that has been performed. Section 5 provides our final remarks.

2. Waveform comparison procedure

The main underlying idea, as explained in [5], is to compare the waveform-agnostic signal reconstruction provided by cWB to the signal models provided by other methods which exploit detailed waveform models. In this Section we will summarize the main points of the general approach, aiming to easy the comprehension of the rest of this note.

In the following, all quantities are referred to the whitened data domain as provided by the cWB methods. On-source data is meant to indicate the data at the GW event time; off-source data indicates data that do not include GW events and provide independent noise replicas of the data.

A signal is reconstructed by cWB as the estimated coherent response of the gravitational wave observatory, separated from the incoherent contributions of each detector, by means of the maximization of a constrained likelihood [2]. The cWB measurement provides a point estimate of the waveform, whose statistical distribution is built by repeating the same analysis on software injections of some signal model performed in off-source data, with a straightforward frequentist interpretation. While each cWB analysis is a wavefrom-agnostic measurement of the signal content in the data, some signal model is needed here to provide the reference hypothesis of the parent distribution of the reconstructed waveforms off-source. As a consequence, this procedure takes into account the actual noise characteristics of the observatory and its statistical results are conditioned to the correctness of the adopted signal model. It is important to notice that the key aspect of this procedure to ensure an unbiased result is the symmetry between the on-source and off-source analyses, in particular it is required that the cWB settings be the same for on-source and off-source measurements. Signals similar to GW190814 are detected with efficiency very close to one, so that the cWB settings for investigating the waveform are standard.

The time-frequency representation of a signal is computed by the Wilson-Daubechies-Meyer (WDM) wavelet transform implemented in cWB [3]. In the following, time-frequency representations refers to the reconstructed signals at each detector, LIGO-Hanford, LIGO-Livingston and Virgo.

For the purpose of comparing waveforms, each measurement consists in the evaluation of the *waveform residual energy*, E_{res}, the sum of squared differences between the waveforms reconstructed by cWB, $W_k^{cWB}(t)$, and a waveform model, $W_k^{model}(t)$, taken as reference, where k indicates the detector and t is time. More specifically, E_{res} is computed in the time-frequency WDM representation of the signal:

$$E_{res} = \sum_{k=1,2,3}^{det} \sum_{i=1,N}^{pixels} (w_k^{cWB}[i] - w_k^{model}[i])^2 \tag{1}$$

where $w[i]$ are the WDM trasforms of the $W(t)$ and the index i denotes the WDM pixels which are part of the cWB reconstruction. [1] There are many other possible choices of test statistic, but measuring the waveform residual energy naturally focuses on the possible discrepancies between the waveform-agnostic reconstruction and the signal model. Moreover, E_{res} proved to be more powerful than e.g. the match factor, in some simulated quests for weak deviations from the signal model.

For a compact binary coalescence event, the signal model is provided by the set of waveform posteriors samples from a parameter estimation procedure based on Bayesian inference under the assumption of Gaussian noise [6, 7]. Assuming the correctness of a specific signal model, the reference distribution of the waveform residual energy E_{res} can be empirically assessed from a simulation, by analyzing software signal injections performed in off-source data at different times. The use of off-source data at different times is necessary to assess the effect of actual noise fluctuations without making assumptions on the noise statistics. In each off-source experiment, a natural choice to compute E_{res} is to use the injected waveform posterior sample as reference w_k^{model} in Eq.(1). Usually the injections are randomly drawn from the set of waveform posterior samples and therefore the resulting off-source distribution of E_{res} takes into account also the uncertainties coming from the signal model. This off-source reference allows to set frequentist confidence intervals on the on-source measurement, assuming the correctness of the signal model. Similarly, the $p-value$ of the on-source E_{res} can be assessed, and a statistical test of the consistency of the on-source cWB reconstruction with the signal model can be performed.

For the on-source measurement of E_{res}, the reference w_k^{model} in Eq.(1) is chosen to be the waveform posterior sample from the parameter estimation procedure which has the maximum likelihood value. Alternative choices are possible among the set of the waveform posterior samples, as e.g. the sample which has the maximum a posteriori probability or even a randomly selected sample. However, we decided to select the maximum likelihood sample since this is the choice that minimizes the squared residuals with the data within the Bayesian inference, and in this sense it is more data-oriented and more homogeneous to the cWB measurement. Both the on-source cWB reconstruction and the bayesian inference are function of the same data, therefore one can expect a positive correlation of the statistical fluctuations between their on-source results and their respective expectation values. This kind of statistical correlation may cause the on-source E_{res} to

[1] for more details see Sec. III.A of [5].

be underestimated with respect to its ideal evaluation based on the true GW signal passing earth, if it were known, which adds a bit of conservativeness to our test of consistency. These expectations are confirmed in simulated conditions [either elaborate or drop]. In any case, the procedure can monitor the distribution of on-source E_{res} resulting from takinf as w_k^{model} in Eq. (1) random draws of the posterior samples from the signal model. However, this kind of bias on the on-ource waveform energy residuals is not expected in the case of the detection of subdominant modes. In fact, as explained in the followning Section, in the latter case, the evaluation of E_{res} is restricted to a portion of the time-frequency representation of the signal for which the considered signal model is null and therefore is not sensitive to the noise of the data pertaining to that portion of the time-frequency volume.

In our current experience, the off-source reference distribution is dominated by the composite effects of non Gaussian noise fluctuations of the data and of measurement uncertainty in the cWB reconstruction. The second contribution in order of relevance comes from the waveform posterior variability of the signal model; instead, the variability of the power spectral density of the data, hence of the whitening filter used at different times, does not significantly affect the results.

3. Determination of the suitable time-frequency portion sensitive to inspiral higher order modes

The test of waveform consistency can be carried out over the full time-frequency volume of the candidate, as detected by cWB. Under this condition, the result is potentially sensitive to the largest variety of possible discrepancies between the reference model for the signal and its morphologically–agnostic reconstruction. However, by inspecting the full detected waveform, the test will be affected by the whole noise uncertainties, which may dilute the significance or distort the reconstruction of a possible deviation. In case the scientific target is more specific, one can take advantage of the available prior information to focus the test within a smaller time-frequency volume. In fact, it is worth trying to tailor a time-frequency volume to be sensitive enough to the target while at the same time less affected by the noise.

This Section describes suitable time-frequency volumes for searching overtones and undertones of the dominant chirp emission during the inspiral of compact binary coalescences. In particular it discusses the procedure that has been implemented to optimize the tailoring of such time-frequency regions, including the choice of the time-frequency resolution of the WDM representation.

A natural descpription of effects from possible subdominant modes, overtones and undertones, can be made in terms of frequency tracks centered at $\alpha \times f_{22}(t)$, where $f_{22}(t)$ is the prediction for the instantaneous frequency corresponding to the dominant mode, $(l = 2, m = 2)$, and α is a dimensionless parameter [10, 11]. Subdominant modes at m are then predicted to have a time-frequency track corresponding to $\alpha \simeq m/2$. A suitable a priori parametrization of the relevant *time-frequency slice* can then be as follows, see Fig. 1:

- include an evolving frequency band defined as $[\alpha-\delta\alpha, \alpha+\delta\alpha]\times f_{22}(t)$ Hz. This is centered on a given α–track and shows a fixed relative half width $\delta\alpha$, which is motivated both to provide a tolerance with respect to the modeled frequency evolution of subdominant modes and to take care of the finite resolution of the cWB time-frequency representation.

- limit the analyzed time range within $[t_{merger} - \Delta t, t_{merger} - \delta t]$ s. Δt is motivated by the robust expectation that subdominant modes may provide their strongest effects in the late inspiral phase only; δt is instead necessary to excise effects related to the merger phase which would leak into the inspiral time range because of the finite resolution of cWB.

- scan over an α range able to cover expected and unexpected contributions from subdominant modes, e.g. over grid values $0.5 - \delta\alpha < \alpha < 3 + \delta\alpha$ with step $\leq \delta\alpha$. This will result in multiple measurements, correlated by the partial overlap of the time frequency slices. The final results as a function of α will contain an effective trial factor. Since all predictions agree that it is the $m = 3$ subdominant mode that generates the strongest effect, it is wise to discuss separately the measurement at $\alpha = 1.5$.

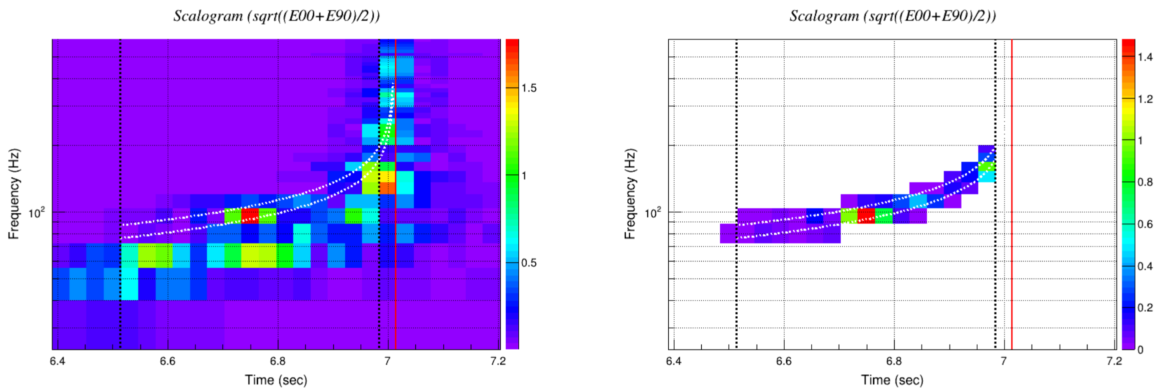

Figure 1: Time-frequency representation of the waveform residual energy of GW190814 in whitened data as measured by cWB, projected into the LIGO Livingston detector using the WDM transform with resolution $dt = 1/32$ s and $df = 16$ Hz. Left: representation of the full time-frequency volume for the cWB reconstruction of GW190814, used to evaluate E_{res}. Right: same but selecting the only time-frequency pixels which are included or partially overlapped with the time-frequency slice which is relevant for the detection of the $m = 3$ subdominant mode. These selection of pixels is used for the evaluation of $E_{res:TF}$. The red vertical line shows the merger time from the maximum likelihood `SEOBNRv4_ROM` waveform posterior. The dotted black vertical lines show the selected time range of the time-frequency slice, $[t_{merger} - 0.5 \text{ s}, t_{merger} - 0.03 \text{ s}]$. The white dotted curves show the selected frequency band of the time-frequency slice, $[\alpha - 0.1, \alpha + 0.1] \times f_{22}(t)$ Hz.

The final waveform residual energy, $E_{res:TF}$ is built as defined by equation (1), with the restriction of summing over the only WDM pixels which pertain to the above described time-frequency slice. For the pixels which are partially included, their contributions to the waveform energy residual are weighted proportionally to the fraction of the pixel area occurring inside the time-frequency slice. This mitigates effects related to the finite time-frequency resolution of the WDM representation, and adds some correlation in the results from disjoint but adjacent time-frequency slices.

The optimization of the shape of the time-frequency slice has been carried out by performing simulations of the measurement for the case $\alpha = 1.5$, i.e. detection of the $m = 3$ multipole, using data around the event time (off-source data). The optimization is based on measurements of the Receiver Operating Characteristic (ROC) [8], with the goal to select the setting which ensures the best balance between the rates of true positives (detection efficiency) vs false positives (false alarm probability) as a function of the test statistics $E_{res:TF}$. Montecarlo simulations in off-source data are implemented by injecting waveform posterior samples randomly drawn from the sets produced by Bayesian inference. [2] The measurements therefore explore both waveform uncertainties from the model and the actual noise statistics of the data and of the cWB reconstruction.

Aligned-spin Effective One Body waveform models without higher modes (`SEOBNRv4_ROM`) and with higher modes (`SEOBNRv4HM_ROM`) [12] have been used to measure respectively the false alarm probability and the detection efficiency as a function of the measured waveform residual energy in the time-frequency slice, $E_{res:TF}$. The false alarm probability at $E_{res:TF}$ is computed as the fraction of simulations from the null model (without higher order modes) that show a waveform residual energy greater or equal to $E_{res:TF}$, where the reference distribution is evaluated from the `SEOBNRv4_ROM` injections and the waveform residual energy is evaluated from the cWB reconstruction and the injected waveform. The detection efficiency at $E_{res:TF}$ is instead computed from `SEOBNRv4HM_ROM` injections, which provide the alternative model. In this case, the waveform residual energy is evaluated from the cWB reconstruction and the injected waveform posterior from the `SEOBNRv4HM_ROM` model, but after switching off its higher order mode emission, thus converting it to a waveform sample of the null model.

Figure 2 shows the ROC using a few variants of the tested settings defining the time-frequency slice, i.e. the parameters df, frequency resolution of the WDM representation, $\delta\alpha$, Δt. Each simulation consisted in thousands of injections. The Receiver Operating Characteristic resulted weakly dependent on variations of the settings around our initial guess (df = 16 Hz, $\delta\alpha = 0.15$, $\Delta t = 0.5$ s). Tested settings inlcuded $df = 8, 16, 32$ Hz, $\delta\alpha$ from 0.05 to 0.4, Δt from 0.2 to 0.6 s. The final choice of the time-frequency portion from the ROC optimization is $df = 16$ Hz, $\delta\alpha = 0.1$, $\Delta t = 0.5$ s. The choice of $\delta t = 0.03$ s has instead been driven to match the time duration of one pixel, in order to avoid to include significant contributions from the merger time, while at the same time it preserves the optimal ROC.

Some figures of merit of this experiment can be easily extracted from the ROC: the cWB detection of the $m = 3$ mode in GW190814, as described in the `SEOBNRv4HM_ROM` waveform posterior set, is expected to give a false alarm probability less than 1% (5%) for about 18% (40%) of the times. This means that this experiment has an interesting probability of detecting the $m = 3$ mode and so it should be pursued. Since the optimization of the time-frequency slice has been carried out usign only off-source data and with simulated signals, it does not pose any condition to the significance of the on-source results, e.g. no trial factors will be required by this optimization.

4. Performances of the method

The results related to GW190814 are presented in [4]. Here we give a deeper look to their interpretation and discuss some relevant checks that have been performed. We first discuss the measurement of the $m = 3$ subdominant mode and then the results for the entire range of tested central α values.

Figure shows the GW190814 on-source result for $E_{res:TF}$ over its off-source distributions in the case of the time-frequency slice centered at $\alpha = 1.5$. It is evident that the on-source result is an outlier of the null model, `SEOBNRv4_ROM`, with a $p - value = 0.0068$. On the contrary, the on-source $E_{res:TF}$ is compatible to a random draw from the signal model including higher order modes, `SEOBNRv4HM_ROM`.

The same measurement has been repeated scanning the central α values from 0.4 to 3.3 in steps of 0.05. The ROC corresponding to the detection of the $m = 1, 4, 5$ modes are compared in Figure 4

[2] the posterior samples are publicly available as supplementary material of [4].

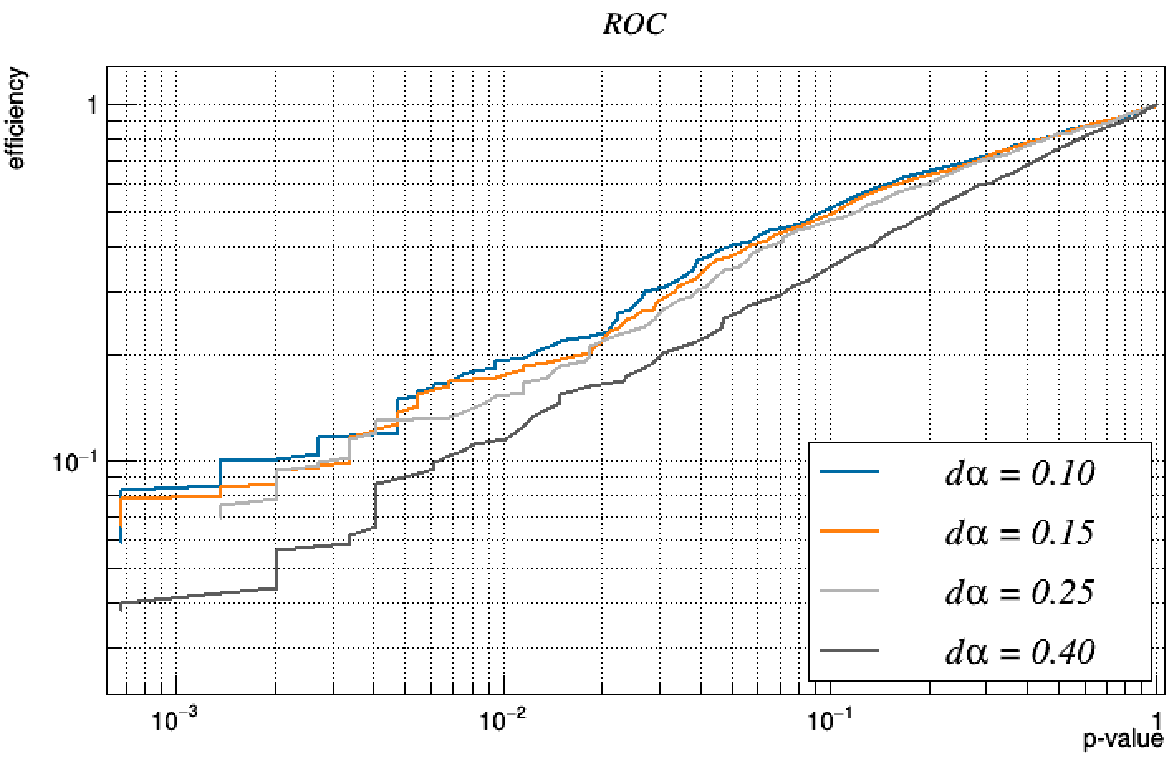

Figure 2: Samples of Receiver Operating Characteristic for different choices of the $\delta\alpha$ parameter, with $df = 16$ Hz and $\Delta t = 0.5$. The optimal settings correspond to the upper curve.

with the ROC of the $m = 3$ detection: the performances of this method for the former set of modes is far from what is achieved for the latter (assuming that nature obeys to the SEOBNRv4HM_ROM signal model). It is also evident that in the case of $m = 1, 5$ modes of GW190814, this method is not performing significantly better than a blind random choice, which would be represented by a bisector of the quadrant. However, the motivation to scan over a wide range of α values using a waveform agnostic search is still valid, to exclude unexpected energy in subdominant modes, in excess to the SEOBNRv4HM_ROM signal model.

Reference [4] reports the $E_{res:TF}$ $p-value$ vs α plot for the null hypothesis, represented by the SEOBNRv4_ROM signal model. There are no significant discrepancies with respect to the null model apart from the $m = 3$ mode, which means that we could not reject the SEOBNRv4_ROM predictions at for $\alpha \neq 1.5$. In particular, cWB detects a dominant $m = 2$ mode consistent with the SEOBNRv4_ROM signal model, leading to waveform energy residuals consisten with noise for $\alpha \sim 1$.

The expected variety of the $p - value$ dip for $E_{res:TF}$ around $\alpha = 1.5$ is visualized in Fig. 5, which shows three $p - value$ curves from the simulation performed to measure the detection efficiency. In particular, these three curves have been randomly selected imposing the condition $p - value < 0.01$ for $\alpha = 1.5$. They approximately represent 18% of the full set of results from the injections in off-source data of waveform posteriors from the SEOBNRv4HM_ROM signal model. Both the position of the $p - value$ minimum and the width of the dip vary according to the different noise features encountered by cWB. Results from further simulations, e.g. by injecting the same waveform posterior either from SEOBNRv4HM_ROM or SEOBNRv4_ROM signal models at different off-

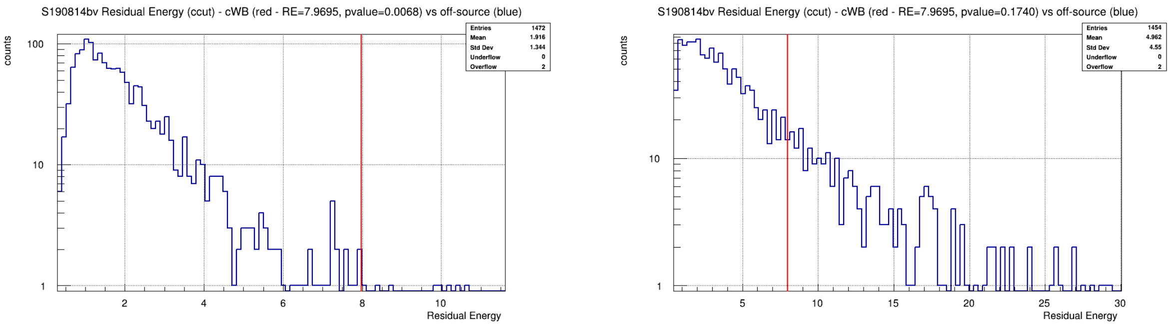

Figure 3: Waveform residual energy for the time-frequency slice centered at $\alpha = 1.5$. Red vertical line: on-source result for GW190814. Left: reference distribution of the null model from `SEOBNRv4_ROM` injectionsin off-source data. Right: reference distribution for the model with higher order modes, from `SEOBNRv4HM_ROM` injections in off-source data. The GW190814 result is an outlier of the null model and instead is compatible with the alternative model.

source times, show that the dominant source of fluctuations comes from the composite effect of non Gaussian noise in the data and of cWB reconstruction uncertainties.

To investigate the expected $p-value$ vs α curves in case inspiral higher order modes were absent in the signal, a few additional injections were performed off-source within 30 s of the GW190814 time from the `SEOBNRv4_ROM` model, see Figure 6. The frequent appearance of weak dips of $p-value$ is driven by the effective trials factor due to the scan along α. The number of disjoint time-frequency slices needed to cover the scanned α range, fifteen, sets un upper limit to the trials factor. Furthemore, the correlation in $E_{res:TF}$ due to pixels overlapping across adjacent slices lowers the expected trial factor. In fact, the $p-value$ curves in Fig. 6 are consistent with an effective trials factor $n \sim 10$: by assuming this value, the estimated probability that an injection from the `SEOBNRv4_ROM` signal model does not show any $p-value$ dip below 5% (10%) in the plot is of the order $0.95^n \sim 0.6$ ($0.90^n \sim 1/3$), which is consistent with what it is shown.

5. Conclusions and final remarks

This method for the detection of inspiral higher order modes in compact binary coalescences has been exploited in the discovery paper on GW190814 [4]. In particular, for GW190814 we measure a $p-value = 0.0068$ for a signal model with null subdominant mode emission at $m = 3$. This method stems from our previous work [5] and implements a new procedure to include robust a priori information on the specific feature of the gravitational wave transient searched for. This is accomplished by focusing the coherent analysis of the data of the network of gravitational wave detectors to a specific portion of the time-frequency representation of the signal, selected by optimizing the Receiver Operating Characteristic. It provides a complementary procedure with respect to the signal energy stacking method described by [10], whose results has been included in the GW190412 and GW190814 discovery papers [11, 4]. In fact, the latter method is based on the analysis of a single detector, on the use of analytical models and on a Gaussian noise assumption, even though it exploits an off-source calibration of the noise variance.

The main underlying idea is to test the consistency between the measurements performed by the waveform-agnostic signal reconstruction over the gravitatioanal wave observatory and the parametric estimates or predictions for the signals based on detailed waveform models, as provided e.g. by Bayesian inference. In particular, this method uses the coherentWaveBurst analysis [2,

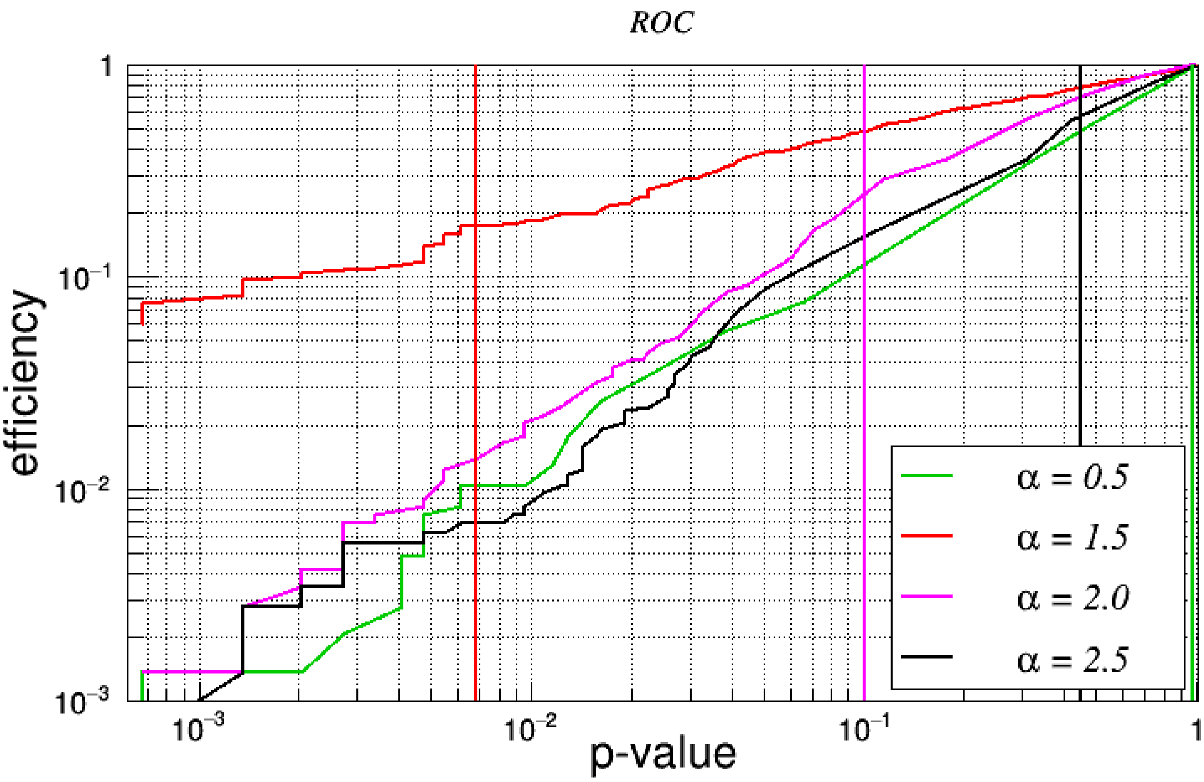

Figure 4: Comparison of Receiver Operating Characteristics for the detection of $m = 1, 3, 4, 5$ modes (green, red, magenta and black curves respectively). The ROCs assume a signal model given by the `SEOBNRv4HM _ROM` set of waveform posteriors. The performance of this experiment in the case of $m = 3$ is by far better than the performances for the other modes. In particular for $m = 1, 5$ the ROC are similar to a blind random choice, which means that the experiment would be informative only in the case of unexpected higher energy in the $m = 1, 5$ modes. Vertical lines show the on-source $p - values$ with the same color code.

9] and its peculiarity is to be able to directly measure the composite uncertainty coming from the observations and from the signal model. This is accomplished by extensive simulations of order thousands of off-source repetitions of the experiment. The final results can be expressend as frequentist $p - values$ or confidence intervals for the on-source measurement, assuming the correctness of the signal model. In particular, the method does not make any assumption on the noise statistics of the data and, in fact, our current experience shows that the dominant source of statistical fluctuations comes from the composite effect of non Gaussian noise in the detectors' data with the uncertainties in the coherentWaveBurst reconstruction.

These procedures can be extended to analyse other different features of gravitational wave transients whose time-frequency representation is understood a priori and therefore a time-frequency region can be tailored to the scope. Applications could include the investigation of features in the spectra or in the luminosity profiles, of post-merger emissions, precursors, memory effects. Work is in progress to develop more of these capabilities and test them on actual observations.

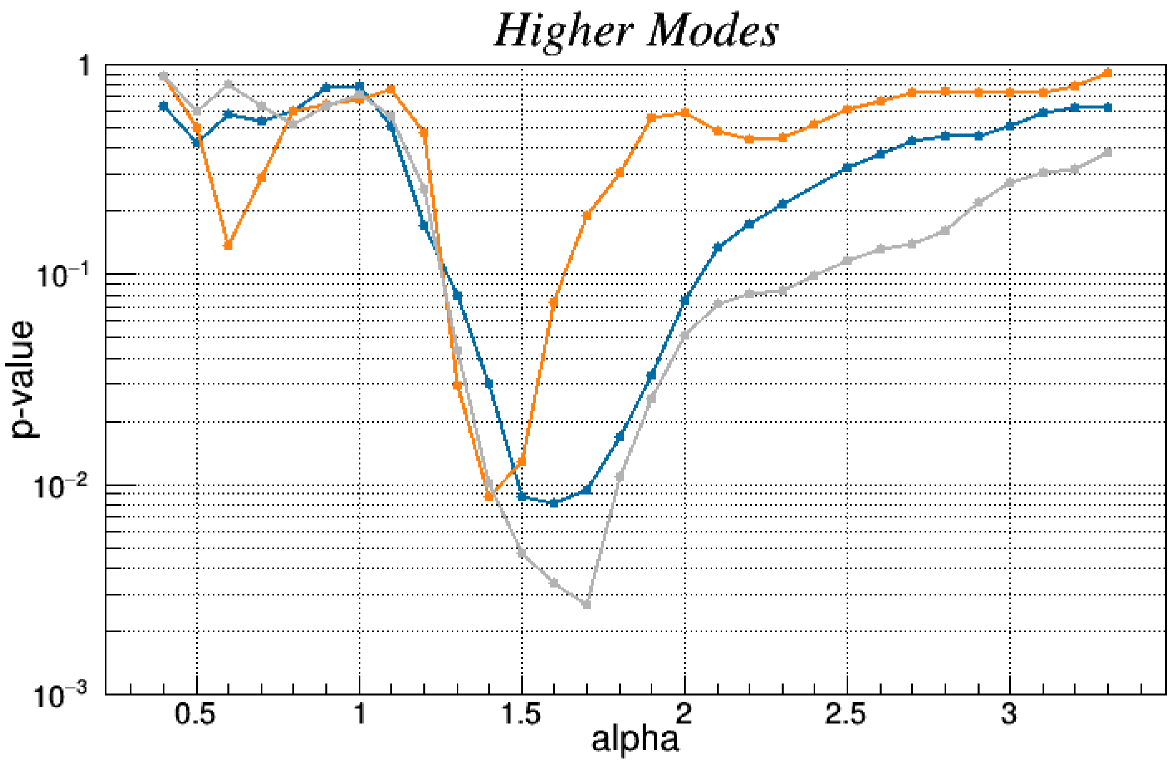

Figure 5: Simulated p-value curves selected from the off-source injections of waveform posteriors from the `SEOBNRv4HM_ROM` signal model. The selection is made under the requirement $p - value < 0.01$ for $\alpha = 1.5$ (they represent 18% of the full set). These cases give a sense of the expected variety of the $p - value$ dip around $\alpha = 1.5$.

Acknowledgements

The authors are grateful for computational resources provided by the LIGO Laboratory and supported by National Science Foundation Grants PHY-0757058 and PHY-0823459. ST is supported by University of Zurich Forschungskredit Nr. FK-19-114 and Swiss National Science Foundation.

[1] B. P. Abbott, R. Abbott, T. D. Abbott, S. Abraham, F. Acernese, K. Ackley, C. Adams, V. B. Adya, C. Affeldt, M. Agathos, et al., A guide to ligovirgo detector noise and extraction of transient gravitational-wave signals, Classical and Quantum Gravity 37 (5) (2020) 055002. `doi:10.1088/1361-6382/ab685e`.
URL `http://dx.doi.org/10.1088/1361-6382/ab685e`

[2] S. Klimenko, G. Vedovato, M. Drago, F. Salemi, V. Tiwari, G. Prodi, C. Lazzaro, K. Ackley, S. Tiwari, C. Da Silva, et al., Method for detection and reconstruction of gravitational wave transients with networks of advanced detectors, Physical Review D 93 (4). `doi:10.1103/physrevd.93.042004`.
URL `http://dx.doi.org/10.1103/PhysRevD.93.042004`

[3] V. Necula, S. Klimenko, G. Mitselmakher, Transient analysis with fast Wilson-Daubechies time-frequency transform, J. Phys. Conf. Ser. 363 (2012) 012032. `doi:10.1088/1742-6596/363/1/012032`.

[4] LVC, Gw190814: Gravitational waves from the coalescence of a 23m
black hole 4 with a 2.6m
compact object (2020).

[5] F. Salemi, E. Milotti, G. A. Prodi, G. Vedovato, C. Lazzaro, S. Tiwari, S. Vinciguerra, M. Drago, S. Klimenko, Wider look at the gravitational-wave transients from gwtc-1 using an unmodeled reconstruction method, Phys. Rev. D 100 (2019) 042003. `doi:10.1103/PhysRevD.100.042003`.
URL `https://link.aps.org/doi/10.1103/PhysRevD.100.042003`

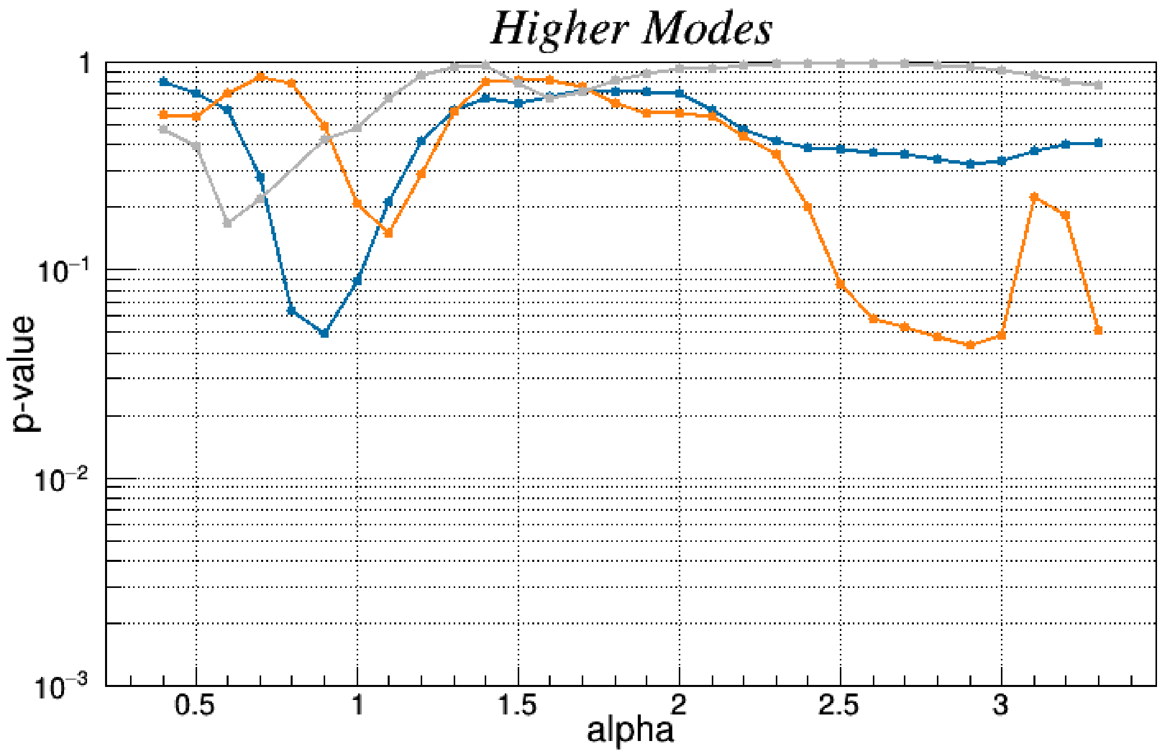

Figure 6: Simulated $p - value$ curves from three additional off-source injections of waveform posteriors from the null signal model, `SEOBNRv_ROM`, performed within 30s of GW190814. The presence of weak dips in the $p - value$ is consistent with an effective trials factor of order 10.

[6] J. Veitch, V. Raymond, B. Farr, W. Farr, P. Graff, S. Vitale, B. Aylott, K. Blackburn, N. Christensen, M. Coughlin, et al., Parameter estimation for compact binaries with ground-based gravitational-wave observations using the lalinference software library, Physical Review D 91 (4). `doi:10.1103/physrevd.91.042003`. URL `http://dx.doi.org/10.1103/PhysRevD.91.042003`

[7] G. Ashton, M. Hbner, P. D. Lasky, C. Talbot, K. Ackley, S. Biscoveanu, Q. Chu, A. Divakarla, P. J. Easter, B. Goncharov, et al., Bilby: A user-friendly bayesian inference library for gravitational-wave astronomy, The Astrophysical Journal Supplement Series 241 (2) (2019) 27. `doi:10.3847/1538-4365/ab06fc`. URL `http://dx.doi.org/10.3847/1538-4365/ab06fc`

[8] T. Fawcett, An introduction to roc analysis, Pattern Recognition Letters 27 (8) (2006) 861 – 874, rOC Analysis in Pattern Recognition. `doi:https://doi.org/10.1016/j.patrec.2005.10.010`. URL `http://www.sciencedirect.com/science/article/pii/S016786550500303X`

[9] cWB team, coherent waveburst, a pipeline for unmodeled gravitational-wave data analysis (2020).

[10] S. Roy, A. S. Sengupta, K. G. Arun, Unveiling the spectrum of inspiralling binary black holes (2019). `arXiv:1910.04565`.

[11] LVC, Gw190412: Observation of a binary black hole with asymmetric masses (2020).

[12] R. Cotesta, A. Buonanno, A. Bohé, A. Taracchini, I. Hinder, S. Ossokine, Enriching the symphony of gravitational waves from binary black holes by tuning higher harmonics, Phys. Rev. D 98 (2018) 084028. `doi:10.1103/PhysRevD.98.084028`. URL `https://link.aps.org/doi/10.1103/PhysRevD.98.084028`